Experimental bulk electronic properties of ferromagnetic iron

A. M. Turner, A. W. Donoho, and J. L. Erskine

Department of Physics, University of Texas, Austin, Texas 78712

(Received 21 July 1983)

Angle-resolved photoelectron spectroscopy utilizing synchrotron radiation has been used to determine the exchange splitting, band dispersion, band symmetries, and critical-point binding energies of ferromagnetic Fe. The magnetic ground-state electronic structure of Fe determined by recent *ab initio* calculations appears to be in good agreement with the results of our photoemission measurements. Correlation effects do not play a major role in influencing the *d*-band width and exchange splitting of Fe determined by photoemission (as appears to be the case for Ni); however, these effects are significant. Introduction of a Coulomb correction to calculated ground-state energies yields improved agreement with our photoemission results. Certain crystal faces and photon energies present experimental difficulties in studying bulk initial-state bands. In these instances, surface effects play an important role in the photoemission processes. These results show that the procedures and approximations, in particular the local exchange and correlation potentials, which have yielded accurate electronic structure models for nonmagnetic *d*-band metals, such as copper, are also able to yield accurate results for a ferromagnetic *d*-band metal.

I. INTRODUCTION

A great deal of effort has recently been directed toward calculating the bulk electronic properties of metals[1-11] and experimentally checking these calculations.[12-22] Such efforts are important for a number of reasons. The bulk electronic properties of metals not only provide the basis for understanding a broad range of physical phenomena associated with condensed matter (optical, magnetic, thermal, transport, and metallurgical properties, for example), but also provide an important starting point for theoretical and experimental studies of surface and interface phenomena which have broad technological importance. Excellent progress has been made in improving theoretical techniques used to calculate the electronic properties of metals. Significant advances have also been made in implementing new experimental methods, particularly angle-resolved photoelectron emission using synchrotron radiation, which can provide a direct probe of the electronic properties of condensed matter and condensed-matter surfaces.

Important issues remain to be addressed in improving our understanding of the experimental methods which probe electronic properties and the approximations used in theoretical models. The issues are fundamental, and are clearly identified by the difficulty encountered in reconciling the best theoretical predictions with recent experimental results. Extensive work on Ni and Cu illustrates some of these issues. The calculated ground-state electronic structure of Cu (Refs. 1—3) and the results of angle-resolved photoelectron-emission studies of Cu single crystals[13-15] are in good agreement. Burdick's calculation[2] for Cu based on Chodrow's potential with nonlocal exchange in the atomic cell appears to have yielded best agreement with experimental results. Results obtained by Moruzzi *et al.*[1] based on the local-density approximation with Kohn-Sham exchange are also in good agreement

with experimental results, but with slightly larger discrepancies. In contrast, corresponding experimental[16,17] and theoretical results obtained for Ni using similar techniques fail to agree in many important respects. Primary discrepancies include a measured *d*-band width 30% smaller than that predicted by one-electron theory and a measured exchange splitting approximately 50% of the predicted value.

More recent theoretical[23-25] and experimental[26-29] work involving spin-polarized photoelectron-emission techniques has permitted the effects of magnetic ordering to be included in the analysis of these discrepancies. Issues being considered in relation to disagreements between experimental results and theoretical predictions include many-body effects,[30,31] the influence of relativistic dipole selection rules,[32] the role played by magnetic surface states,[33,34] and the approximations inherent in ground-state electronic structure calculations.[35-37] At present, these discrepancies are generally regarded as significant and remain to be adequately explained.

Electronic structure calculations using the one-electron approximation are based on simplifying assumptions which include the local-density approximation of electronic exchange and correlation[35,36] and the muffin-tin approximation.[37] Most calculations also neglect relativistic effects. Present disagreements between various calculations and between theory and experiment are believed to result primarily from the one-electron potential which is used in the calculations. In addition to the numerical approximations inherent in the muffin-tin form of the crystal potential, the most serious uncertainty is believed to be in the contribution to the potential which describes the interaction between electrons. The degree to which a specific one-electron potential approximates many-particle systems and its best functional form for those systems which are accurately described has not been established.

In addition to the factors which only affect theoretical

predictions, other factors enter into the picture when theoretical calculations are compared with experiment. It is important to stress the fact that photoemission experiments measure the excitation spectrum of a solid whereas in a calculation, in general, the ground-state eigenvalue spectrum is determined. Ground-state energies based on local-density approximations will, in principle, not agree with single-particle excitation energies. At present, the extent to which correlation effects enter into the interpretation of binding energies, measured by photoemission in terms of calculated ground-state energies, has not been well established. Also, it is worth noting that, at present, there are no broadly successful theories which permit accurate interpretation of photoemission intensities. These points must be considered in comparing photoemission results with ground-state calculations.

We have chosen to investigate Fe because there are several calculations of its electronic properties and because it is closely related to Ni in terms of both electronic and magnetic properties. Very few photoemission studies of Fe single crystals have been reported.[18-22] Heimann and Neddermeyer[18] conducted angle-resolved photoemission studies of the (100), (111), and (110) crystal faces of Fe at photon energies of 11.83, 16.85, and 21.22 eV. They concluded that most of the emission features were consistent with the calculated density of states for Fe, but were unable to directly obtain critical-point binding energies, band dispersion, or the exchange splitting. Kevan et al.[19] and Schultz et al.[20] also encountered difficulty in accounting for angle-resolved photoemission spectra obtained from single-crystal surfaces of Fe in terms of calculated bands based on a direct-transition model. Eastman, Himpsel, and Knapp[21] reported angle-resolved photoemission measurements for Fe(111) using synchrotron radiation which established the binding energies of the $P_{3\uparrow}$, $P_{4\downarrow}$, and $P_{4\uparrow}$ bands along the Λ direction of the bulk Brillouin zone. Eastman et al. also determined the exchange splitting at P ($E_{P_{4\uparrow}} - E_{P_{4\downarrow}} = 1.5$ eV).

In this paper we present extensive angle-resolved photoemission results for Fe surfaces. Based on the direct-transition model for photoemission, we obtain critical-point binding energies, band dispersion and symmetries, and the magnetic exchange splitting at several points in the three-dimensional Brillouin zone. We conclude from our photoemission results that state-of-the-art calculations based on local exchange and correlation potentials yield accurate ground-state energies, exchange splitting, and band dispersion. Measured binding energies for Fe agree with calculated ground-state energies to an accuracy of about 10% in contrast to the 30% discrepancy found for Ni. Based on this it is clear that correlation effects do not play a dominant role in determining the ground-state energies from photoemission. Correlation effects are significant, however, because introducing a correction for these effects reduces the 10% discrepancy between calculated and measured energies to less than experimental uncertainty.

II. EXPERIMENTAL CONSIDERATIONS

Our experiments were conducted at the Synchrotron Radiation Center in Stoughton, Wisconsin, using the stainless-steel Seya Namioka monochromator and an angle-resolving photoelectron spectrometer. The spectrometer consists of an angle-resolving electron-energy analyzer mounted on a two-axis goniometer in a main chamber which is coupled via a gate valve to a sample preparation chamber which contains low-energy-electron diffraction (LEED) optics and Auger analysis capability. The goniometer permits the analyzer to be oriented along any axis through the target point. Samples are inserted into the main chamber from the preparation chamber by a manipulator which has a translational axis in the plane of incidence and perpendicular to the beam of light from the monochromator. The manipulator permits 360° rotation around the translation axis and a 120° tilt of the sample around an axis perpendicular to the manipulator translation and/or rotation axis. The combination of sample- and electron-analyzer motions permits all polar detection angles to be investigated for s-polarized light incident at angles greater than 30° and mixed ($s + p$)-polarized light incident at angles greater than 10°. Figure 1 defines the angular parameters used in describing polarization, angle of incidence and emission angles, and illustrates the sample manipulator functions described above.

Our photoelectron spectrometer, including the electron optics, was designed specifically for synchrotron-radiation work. A complete description of the spectrometer is given elsewhere,[38] and we have previously reported comprehensive tests of the electron optics.[39,40] The electron-energy analyzer is a Kuyatt-Sympson design based on hemispherical energy dispersing elements coupled to input and output lenses and angle-defining aperatures which permit photoemission spectra to be taken at constant angular resolution, constant energy resolution, and unity spectrometer transmission. All of the spectra reported here were taken at approximately 100-meV resolution (limited by the slit settings of the Seya monochromator) and angular resolution of ±1.2°.

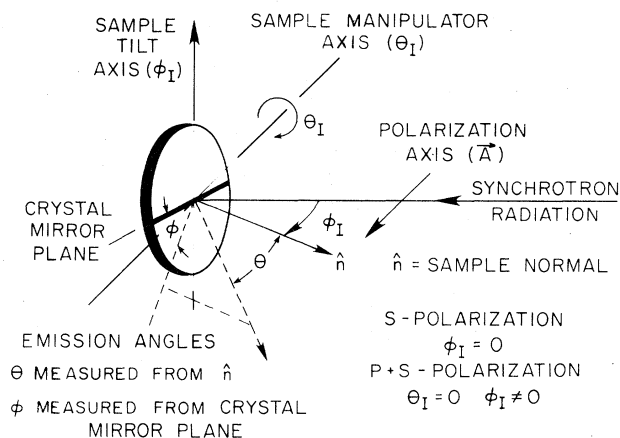FIG. 1. Sample geometry: θ_I and ϕ_I are angles between the sample normal vector $\hat{n}$ and the synchrotron-beam direction in a plane perpendicular (θ_I) and parallel (ϕ_I) to the polarization vector $\vec{A}$. θ and ϕ define the emission angle with respect to the sample normal (θ) and the crystal-mirror plane (ϕ) which is parallel to $\vec{A}$.

Three high-symmetry crystal faces of Fe were investigated: the (111), (100), and (110) crystal faces. Normal emission from these crystal faces corresponds to bulk initial-state k values along the Λ, Δ, and Σ directions of the three-dimensional Brillouin zone for the bcc iron. The samples were mounted with a crystal-mirror plane along the $\vec{A}$ vector of incident light (see Fig. 1) to permit surface electronic properties to be studied along high-symmetry directions in the two-dimensional Brillouin zone as well as some off-normal emission studies of the bulk bands.

Our Fe signal crystals were spark-cut and aligned to approximately $\pm 1°$ using x-ray Laue techniques and were mechanically polished to mirror surfaces using alumina powder to 0.05-μm size. Bulk impurities were reduced by annealing the cut crystals in a flowing hydrogen atmosphere (10 mol% H_2 + 90 mol% Ar) for several weeks at $\sim 800°C$. Subsequent *in situ* cleaning involved numerous cycles of argon ion sputtering (500 eV 1μA/cm^2) and annealing ($500°C$–$850°C$). Clean surfaces yielded excellent LEED patterns and practically no surface contamination. Trace amounts of oxygen were detected at concentrations corresponding to oxygen Auger peaks (530 eV) about $\frac{1}{10}$ of the intensity of the small Fe peak (562 eV). This ratio indicates an oxygen coverage of a few percent of a monolayer.

Analysis of our photoemission data is based on symmetry selection rules and conservation laws associated with the photoemission process. In normal-emission geometry the detected final state must be symmetric, and for emission in a mirror plane of the crystal only even final states are detected by the analyzer. The photoemission matrix element

$$P_{fi} = \langle \psi_f \,|\, \vec{A} \cdot \vec{p} \,|\, \psi_i \rangle \qquad (1)$$

connects initial- and final-state wave functions (ψ_i and ψ_f) through the vector potential $\vec{A}$ which characterizes the incident radiation. The dipole operator $\vec{A} \cdot \vec{p}$ is even (or odd) if $\vec{A}$ is parallel (or perpendicular) to the mirror plane in which electrons are detected. This leads to the selection rules for initial states shown in Table I.[41,42]

The direct-transition model for photoemission is based on the conservation of energy and of crystal momentum parallel to the surface.[43] We use this model to analyze our photoemission data. The basic conservation laws may be described by the following equations:

$$E_f = E_i + \hbar\omega , \qquad (2)$$

$$E_{\text{kin}} = E_f - e\phi , \qquad (3)$$

$$k_{\|\text{inside}} = k_{\|\text{outside}} , \qquad (4)$$

where $G_\|$ in Eq. (4) denotes surface and bulk reciprocal-lattice vectors parallel to the surface. Equation (2) states that the initial- and final-state band energies differ by the photon energy, Eq. (3) states that the kinetic energy of the detected electron in vacuum, E_{kin}, is equal to the final-state energy minus the metal-surface work function, ϕ, and Eq. (4) states that the component of the crystal momentum parallel to the surface is a conserved modulus, a surface or bulk reciprocal-lattice vector. In photon-energy ranges where the collection geometry and bulk band structure permit direct transitions, contributions to the detected photocurrent are generally dominated by bulk G vectors which couple the initial state to a bulk final band.

The parallel component of detected electron momentum can be obtained directly from the measured electron kinetic energy and its direction:

$$k_\| = \left[\frac{2m}{\hbar^2} E_{\text{kin}} \right]^{1/2} \sin\theta . \qquad (5)$$

In Eq. (5) θ is the emission angle in the detection plane measured from the sample normal. Since parallel momentum is conserved, this expression also gives $k_\|$ of the initial-state modulus appropriate $\vec{G}$ vectors as indicated in Eq. (4). Normal-emission geometry corresponds to $\theta = 0$. The objective of our experiments is to determine the initial-state binding energies as a function of k along high-symmetry lines of the Brillouin zone.

The perpendicular component of momentum, $k_\perp$, is not conserved when the electron escapes from the surface, and $k_\perp$ can only be determined if the dispersion of the final-state band is known or can be determined. There are three commonly used methods for obtaining the final band. One approach is to determine the complete initial-state and final-state band structure experimentally.[43] However, Fig. 2 shows that the calculated band structure for iron presents a reasonably good general picture of the initial- and final-state bulk bands. In the present case, we are interested in determining the initial-state binding energies along high-symmetry lines in the three-dimensional Brillouin zone. We have therefore used the calculated bands as a starting point for our data analysis. A second approach is to use calculated final-state bands (as shown in

TABLE I. Symmetry of initial- and final-state bands probed in normal-emission geometry from the three high-symmetry faces of a bcc crystal.

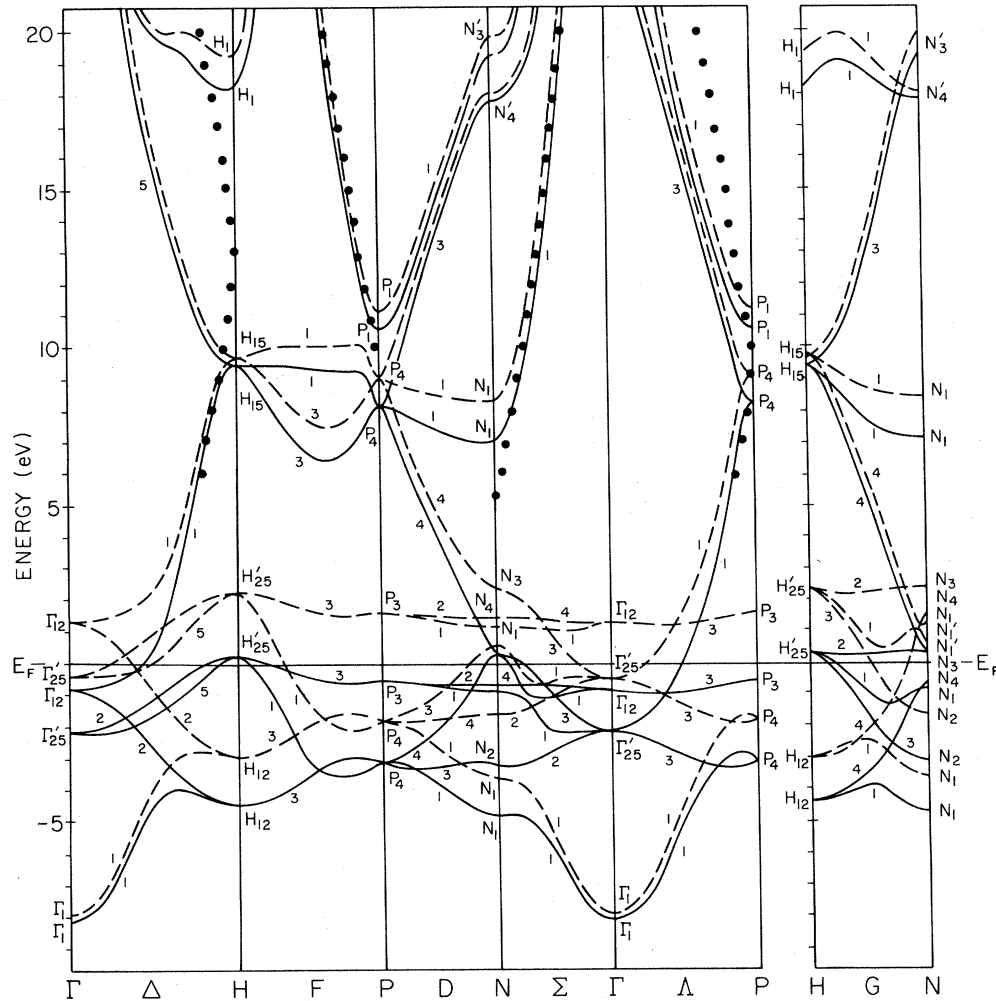| Crystal face	Allowed final state	Initial states		
		s polarization		p polarization
		$A_{\|x}$	$A_{\|y}$	$A_{\|z}$
(100)	Δ_1	Δ_5	Δ_5	Δ_1
(111)	Λ_1	Λ_3	Λ_3	Λ_1
(110)	Σ_1	Σ_3	Σ_4	Σ_1

FIG. 2. Energy bands of ferromagnetic iron calculated by Callaway and Wang (Ref. 7). Solid lines, majority-spin bands; dashed lines, minority-spin bands. Dotted lines along Δ, Σ, and Λ directions represent free-electron final bands used in analysis of photo-emission data (see text).

Fig. 2), and a third approach, which simplifies analysis, is to approximate the final-state bands using a free-electron model. With this approximation the final-state band energy can be described by

$$E_f(k_\perp) = \frac{\hbar^2 k_\perp^2}{2m} + U_0 + e\phi , \tag{6}$$

where $k_\perp$ is related to the kinetic energy by

$$k_\perp = \frac{2m}{\hbar^2}(E_{\text{kin}}\cos\theta + U_0) . \tag{7}$$

In these equations U_0 is the inner potential which places the energy of the free-electron final band in relation to the Fermi energy. Equations (1)–(7) constitute the basis for analyzing both normal- and off-normal[16] photo-emission data using the direct-transition model. We have found that by assuming a free-electron final band to approximate the Δ, Λ, F, and Σ bands above E_F we are able to account for most of the major peaks in photoemission spectra in terms of dipole-allowed transitions. Our experimental data permit us to determine U_0 and accurately

place the final bands. Also, we obtain directly from our data accurate values for final-state bands above E_F at zone edges.

III. EXPERIMENTAL RESULTS

A. Fe(110) normal emission

Figures 3 and 4 display normal-emission angle-resolved photoemission spectra for Fe(110) surfaces obtained with a light polarization vector along the [1$\bar{1}$0] direction. In Fig. 3 the energy-distribution curves (EDC's) correspond to mixed $s + p$ polarization (resulting from $\theta_I = 0$, $\phi_I = 50°$) and in Fig. 4 the EDC's correspond to primarily s polarization ($\theta_I = 0$, $\phi_I = 15$). In a previous paper[22] we reported angle-resolved photoemission studies of Fe(110) using unpolarized light from a resonance lamp. We were able to account for the observed structures in the EDC's in terms of the direct-transition model which used a free-electron final band. The position of the final band was determined by following the peak in the EDC's due to the
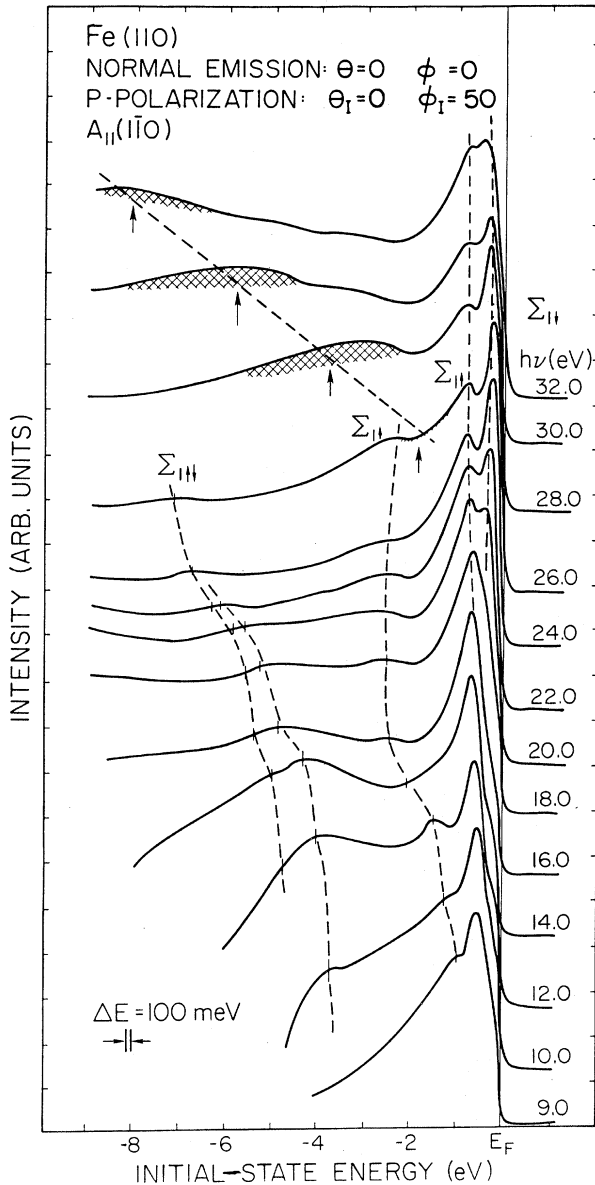
FIG. 3. Normal-emission EDC's for Fe(110). Light is p polarized [$\vec{A}$ along $(1\bar{1}0)$] and incident at 50° from the sample normal. Dashed lines connect structures resulting from Σ_1 (even-) initial-state bands. Arrows and shaded peaks identify final-state resonance structure.
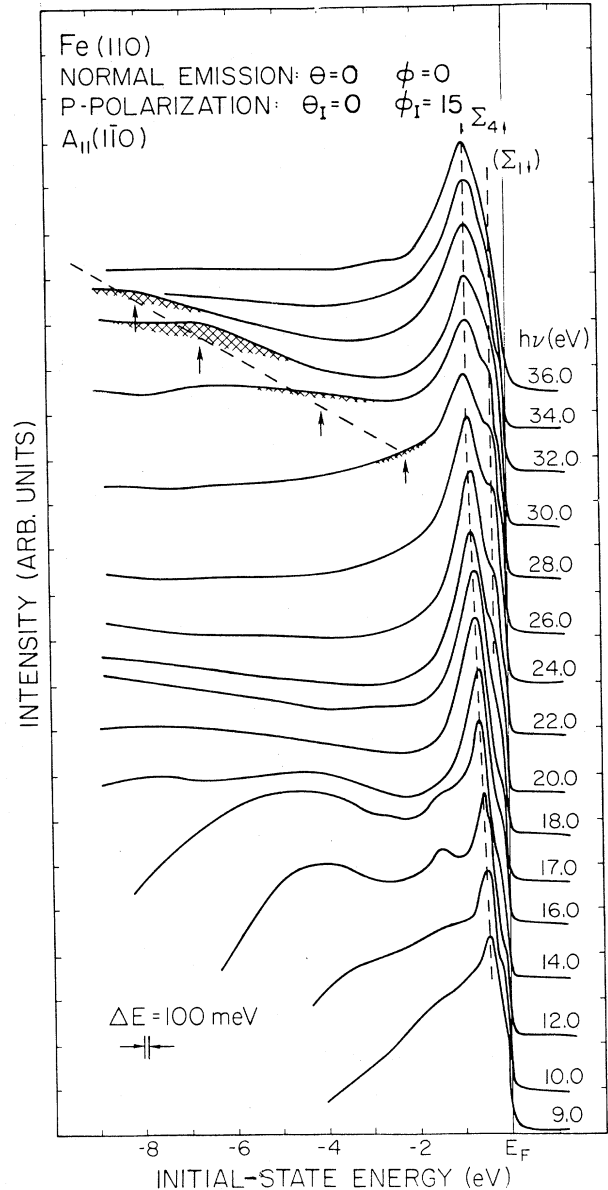
FIG. 4. Normal-emission EDC's for Fe(110). Light is predominantly s polarized [$\vec{A}$ along $(1\bar{1}0)$] and incident at 15° from the sample normal. Dashed lines connect structure resulting from the Σ_4 (odd) initial state. The weak Σ_1 (even-) state feature is due to a small p-polarization component. Arrows and shaded peaks identify the final-state resonance structure.

lower $\Sigma_{1\uparrow\downarrow}(s\text{-}p)$ band to Γ. In this case [normal emission from the (110) surface] the condition $k_\perp=0$ occurs very near the photon energy for He II (40.82 eV).

Using synchrotron radiation we have checked our previous EDC peak assignments by determining the band symmetries (based on Table I) and have added many more experimental points to the $E(k_\perp)$ values along the Σ direction. Figure 5 displays experimental $E(k_\perp)$ points plotted over the calculated band structure[7] along the Σ direction. With the exception of one structure in the EDC's (discussed later) all peaks observed in normal emission from Fe(110) correspond to bulk initial-state bands along the Σ direction. The free-electron final-band energies are indicated along the top of Fig. 5 with corresponding $k_\perp$ values

along the bottom. The free-electron final band shown as large dots in Fig. 2 corresponds very closely to the Σ_1 symmetry band predicted by the calculation. The inner potential for this free-electron band is $U_0=9.35$ eV.

By referring to Fig. 3, the $\Sigma_{1\uparrow\downarrow}$ and lower $\Sigma_{1\uparrow}$ band dispersion can be directly seen in the EDC's for photon energies ranging between 9 and 26 eV. In the photon-energy range between 28 and 32 eV a final-state resonance (identified by arrows), which is discussed in more detail later, obscures these two bands. The EDC's of Fig. 3 show reasonable evidence that the spin splitting of the lower $\Sigma_{1\uparrow\downarrow}$ band can be resolved at $k_\perp$ values near N and values of $k_\perp$ extending to near the center of the zone (for example, at photon energies of 12—16 eV). However, as
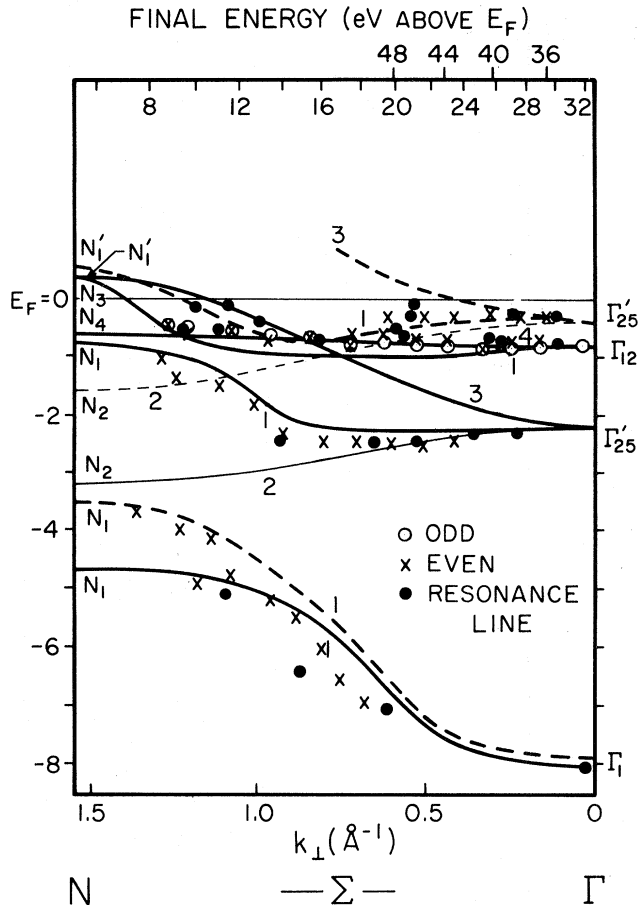
FINAL ENERGY (eV ABOVE E_F)

FIG. 5. Experimental results plotted over calculated bands along the Σ direction for ferromagnetic iron. Binding energies of even states are represented by $\times$, odd states by $\bigcirc$, and states determined using unpolarized light (resonance lamps) by $\bullet$. Initial band $k_\perp$ and the final-band energy above E_F are shown along the bottom and top of the figure.

this band disperses down toward Γ, it loses its d character and the splitting decreases to a value too small to resolve. At higher photon energies not shown in Figs. 3 and 4 (40.82 and 48.38 eV) the final-state resonance does not interfere with the lower $\Sigma_{1\uparrow\downarrow}$ band peak and the Γ_1 point can be accurately determined.

Near the Fermi energy, peaks due to emission from the $\Sigma_{1\uparrow}$ and $\Sigma_{1\downarrow}$ bands can be observed. These peaks are not resolved for photon energies between 10 and 18 eV ($k_\perp$ values between 1.25 and 0.75 Å^{-1}) because the bands lie very close to each other in this range (see Fig. 5). For photon energies above 18 eV, these two bands are clearly resolved and they can be followed to Γ_{12} and Γ_{25} at $k_\perp=0$ which occurs at a photon energy of about 32 eV.

Figure 4 displays EDC's obtained with s-polarized light with polarization along the [1$\bar{1}$0] direction. This geometry permits Σ_4 initial states to be observed (Table I). The primary structure in all EDC's in Fig. 4 is the peak near E_F which exhibits practically no dispersion with photon energy. This structure is due to emission for the $\Sigma_{4\uparrow}$ band. Our EDC's show that this band disperses downward slightly from N to Γ_{12}. The measured $\Sigma_{4\uparrow}$ binding

energy at $k_\perp=1.25$ Å^{-1} (9-eV photon energy) is 0.50 eV. The $\Sigma_{4\uparrow}$ band and the $\Sigma_{1\uparrow}$ band become degenerate at Γ_{12} and both bands ($\Sigma_{4\uparrow}$ is odd and $\Sigma_{1\uparrow}$ is even) can be followed to Γ_{12} and yield a binding energy of 0.78 eV for this point. The Σ_3 bands can be probed with polarization along the [001] direction.

The s-polarization data in Fig. 4 contain a small component of p polarization resulting from the 15° angle of incidence. Refraction effects also help emphasize this component. The p component accounts for evidence of the $\Sigma_{1\uparrow}$ band in EDC's for 12- and 14-eV photon energies and also for the weak shoulder near E_F at photon energies between 22 and 32 eV which is due to emission from the $\Sigma_{1\downarrow}$ band.

We observed a weak structure in both s-polarization and p-polarization EDC's from Fe(110) which is identified in Figs. 3 and 4 by arrows. The binding energy of this peak is approximated by $E_B=\hbar\omega-24$ eV, i.e., the kinetic energy of emitted electrons $E_{\text{kin}}=(24 \text{ eV}-\phi)$ corresponds to a constant final-state energy of $E_f=E_{\text{kin}}+\phi=24$ eV. We attribute this structure to a final-state resonance. The excitation cross section for this resonance (represented by the shaded region under the peak) appears to be largest for photon energies between 28 and 32 eV (approximately 28 eV for p-polarized light and a little higher, 32 eV, for s-polarized light). Corresponding features are observed in generally the same photon-energy range in EDC's from the other iron surfaces.

Energy-loss spectra for iron[44,45] exhibit features which can be explained in terms of both single-particle excitations (i.e., dipole- and quadrupole-allowed transitions) and collective excitations (bulk and surface plasmons). Major energy-loss features observed for iron and identified as orginating from single-particle excitations occur at 2.5, 5.9, 9.1, 12.0, 18.4, and 24.8 eV.[44] The two higher-energy losses also correlate with structure in optical spectra[46] and therefore are due to dipole transitions. In both cases, the optical- and energy-loss spectra are attributed to transitions to the N point in the bulk Brillouin zone. This interpretation is in general agreement with our experimental results.

The bulk band structure in Fig. 2 describes final-state bands to energies about 20 eV above the Fermi energy. Our photoemission data place the Σ_1 final band at N ($N_{1\uparrow\downarrow}$) appreciably below the predicted value ($N_{1\uparrow\downarrow}\sim5$ eV above E_F). For $k_\perp$ values away from N, this band agrees well with the Δ_1 band. Based on the final-state resonance we have observed in photoemission and which has been observed in energy-loss and optical experiments, we predict a final state about 25 eV above E_F at N which should exhibit weak dispersion over an appreciable range of $k_\perp$ values similar to the $H_{1\uparrow\downarrow}$ structure seen at 19 eV, in Fig. 2.

B. Fe(100) normal emission

Figures 6 and 7 display normal-emission photoemission spectra for Fe(100) obtained with the light polarization vector along the [010] direction. Similar data (not shown) were obtained for the polarization vector along the [011] direction. The data of Fig. 6 correspond to pure s polari-
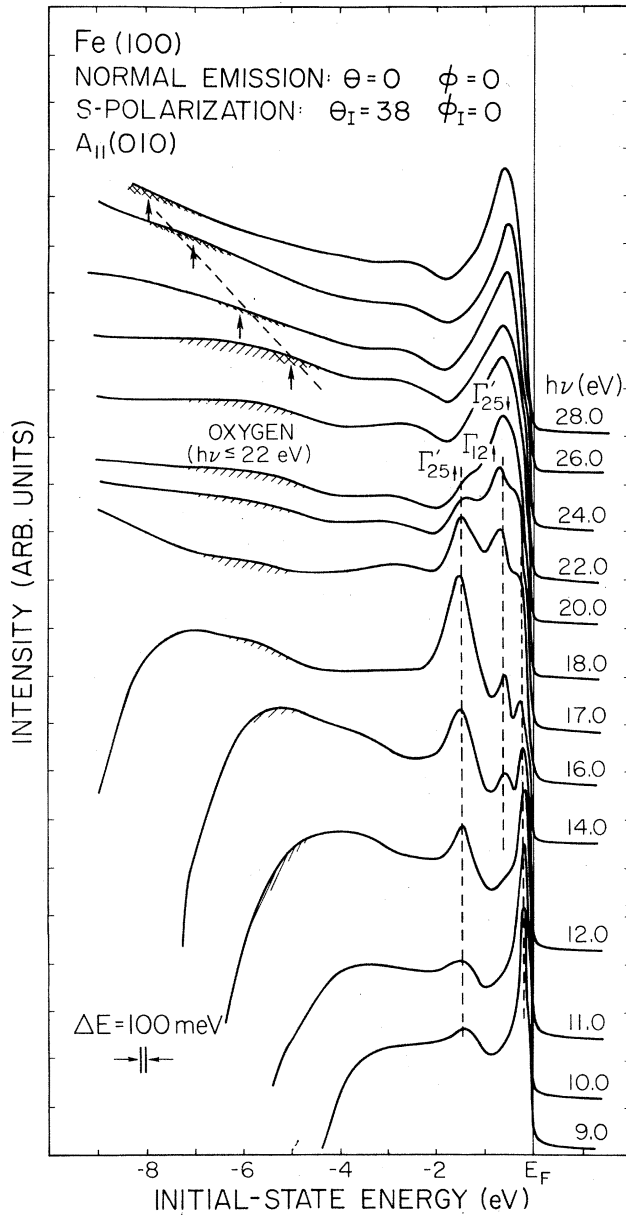
FIG. 6. Normal-emission EDC's for Fe(100). Light is pure s polarized [$\vec{A}$ along (010)] and incident at $\phi_I = 38°$. Dashed lines connect nondispersing peaks originating from transitions near Γ. Light shaded peaks identify oxygen $2p$ levels (see text). Arrows and dark shaded peaks identify final-state resonance structure.
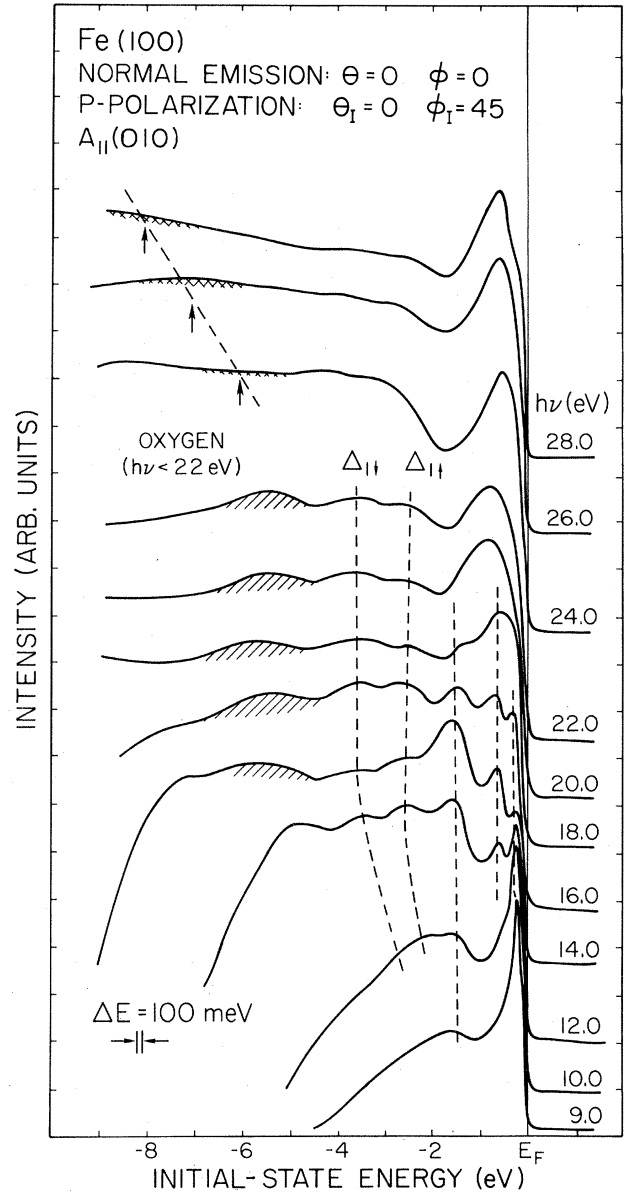
FIG. 7. Normal-emission EDC's for Fe(100). Light is p polarized [$\vec{A}$ along (010)] and incident at $\phi_I = 45°$. Dashed lines connect structures resulting from Δ_1 (even-) state features. Non-dispersing peaks originate from initial states near Γ. Light shaded peaks identify oxygen $2p$ levels (see text). Arrows and dark shaded peaks identify final-state resonance structures.

zation ($\phi_I = 0$, $\theta_I = 38°$) and data in Fig. 7 correspond to mixed $s + p$ polarization ($\phi_I = 45°$, $\theta_I = 0$). Table I indicates that in normal-emission geometry, the final state for emission along the [100] direction must have Δ_1 symmetry and that initial states will have Δ_1 (even) symmetry for p polarization and Δ_5 (odd) symmetry for s polarization.

Figure 2 shows that there is a predicted minority-spin Δ_1 symmetry band which lies above E_F over the entire reduced zone ($k_\perp = 0 - k_\perp = 2.197$ Å^{-1} along Δ) and a majority-spin Δ_1 symmetry band which lies above E_F over about half of the zone ($k_\perp = 1.0 - k_\perp = 2.197$ Å along Δ). These Δ_1 bands are nearly degenerate at H but exhibit an appreciable exchange splitting at Γ. This is a clear exam-

ple where a single free-electron final band is not expected to be very accurate except possibly in the narrow range of $k_\perp$ values near but not at the H point.

This particular region of k space (along the Δ line) also exhibits an interesting feature which is characteristic of the Brillouin zone of bcc metals: There is a large gap predicted in the Δ_1 symmetry final band at H. In the present case, the gap extends from approximately 10 to 20 eV above E_F at the H point. Based on this feature, we expect a photon-energy range over which direct transitions are not allowed and where other photoemission mechanisms should dominate, i.e., surface photoemission. A similar Δ_1 gap above E_F accounts for the strong surface-

state and surface-resonance features observed for $W(100)$ and $Mo(100)$ surfaces.[47]

The Δ_1 symmetry gap at H can be used to determine the final band near H. Direct transitions from $\Delta_{5\uparrow}$ to $\Delta_{1\uparrow}$ are allowed for s-polarized light, and from inspection of Fig. 2, one would expect the emission peak from this state to disappear abruptly near H for two reasons: First, the Δ_5 band crosses E_F close to H, and second, there is a gap in the Δ_1 symmetry final band at H. Normal-emission s-polarization data (Fig. 6) shows that the cross section of the peak nearest to E_F decreases abruptly at a photon energy of 14 eV. This is evidence that the $\Delta_{1\uparrow}$ final-band energy near H is approximately 14 eV above E_F. This permits us to accurately determine the final band used to analyze direct transitions from the (100) surface. The free-electron band is plotted in Fig. 2 (dotted line along Δ direction). We note that this final band is in good agreement with the band we arrived at previously using resonance lamp lines.[22] We have found that surface states and surface resonances play an important role in the photoemission spectra observed from the Fe(100) surface.[48,49] In order to quench emission from surface states and surface resonances and permit bulk features to be studied, we have chemisorbed oxygen (a few tenths of a monolayer) on the surface to obtain EDC's which emphasize bulk bands. This procedure is particularly useful for photon energies below $h\nu=22$ eV where surface states and resonances can dominate the spectra. The oxygen $2p$ levels have binding energies approximately 5.5 eV below E_F, and the emission from these levels is shown in Figs. 6 and 7 by shading the corresponding peaks in the EDC's. Several consistency checks were made to determine the submonolayer oxygen coverages did not significantly shift peaks in the EDC's arising from bulk bands. Surface-state emission is also effectively quenched by argon ion sputtering (500 eV 10 $\mu A/cm^2$ for a few minutes). LEED patterns of the sputtered surfaces consisted of the same (1×1) pattern observed for clean annealed surfaces, but in addition, exhibited a noticeably stronger diffuse background. Peak positions and shapes for the clean disordered (sputtered) surfaces were identical to those for low-coverage oxygen surfaces with the exception of the oxygen $2p$ levels. Peaks in the off-normal EDC's from Fe(100) which resulted from direct transitions were not noticeably affected by the presence of oxygen and changed in the same manner with $k_{\parallel}$ regardless of the presence or absence of oxygen. These tests justify our procedure for quenching surface-state and surface-resonance emission using fractional monolayer oxygen coverages. Our investigation of surface states and surface resonance on iron surfaces will be reported elsewhere.

Referring to Fig. 6, it is clear that all of the peaks in the EDC's corresponding to Δ_5 (odd) initial states exhibit constant binding energy as photon energy is changed. Surface-state and surface-resonance features have been quenched by adsorbed oxygen. The peak at E_F which disappears as photon energy is increased above 14 eV is due to the $\Delta_{5\uparrow}$ band which crosses E_F near H. This peak lies too close to E_F in the photon-energy range where it is observed to accurately determine the $\Delta_{5\uparrow}$ dispersion. The other two major structures result from surface emission

from high density-of-states regions near Γ. The binding energies of these peaks are the same as the values of Γ_{25}' and Γ_{12} deduced from the (110) surface.

We performed several tests to verify that these peaks involve a surface-related mechanism as one would expect for an EDC feature associated with transitions from a bulk state to an evanescent LEED final state. Figure 8 illustrates one example of a surface resonance on Fe(100) and the effects disorder and oxygen chemisorption have on emission from bulk and surface states. The photon energy chosen (16 eV) corresponds to $k_\perp$ near H along the Δ line in k space. The Δ_2 and Δ_5 bands are above E_F at this point, and one does not expect any peaks from direct transitions from the H_{12} levels because there is no Δ_1 final band at this photon energy.

In Fig. 8 one can see a sharp peak just below E_F and a weaker peak corresponding to a binding energy of about
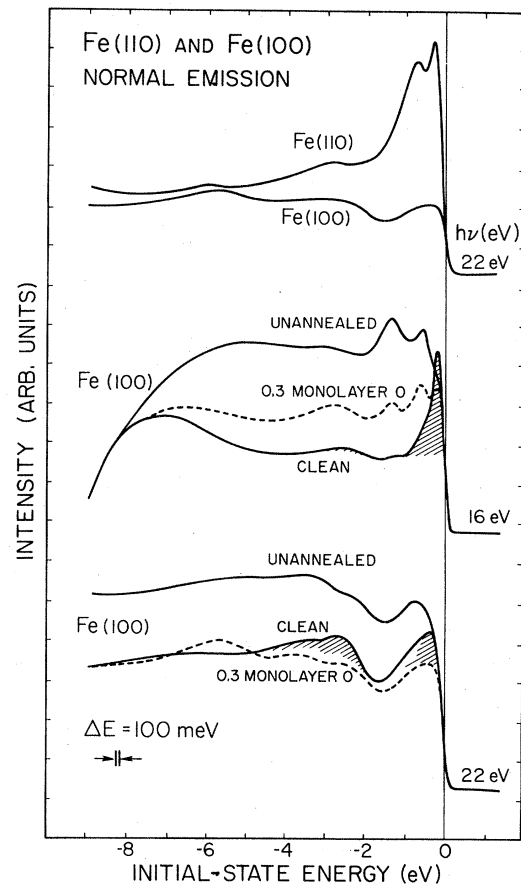

FIG. 8. Top panel contrasts emission intensity at $h\nu=22$ eV for two cases where a final band allows direct transitions [(110) surface] and where no final band is present [(100) surface]. In both cases several initial-state bands lie below E_F. Center and bottom panels display strong surface resonances (shaded areas) observed for a clean (100) surface and the effects of disorder (unannealed) and chemisorption (0.3 monolayer oxygen). Bulk feature binding energies are the same for disordered and chemisorbed surfaces. Center panel corresponds to peak in the surface resonance (at $h\nu=16$ eV) where the final state is a bulk band. At $h\nu=22$ eV, no Δ_1 bulk band is available and the strength decreases.

−3 eV. Gentle sputtering (500 eV, 10 μA/cm^2) quenches the surface emission and simultaneously increases both the secondary-electron background *and* the bulk emission from the Γ_{12} and Γ'_{25} states which arise from the surface-photoemission mechanism. Adsorption of a 0.3 monolayer of oxygen also quenches the surface features and enhances both the background and surface emission from the bulk Γ_{12} and Γ'_{25} states. All three spectra have been normalized (to account for the storage-ring beam current and number of analyzer sweeps) and therefore reflect the relative emission intensities of the spectra. It is interesting to note that the clean well-ordered surface exhibits surface-state emission, but the total integrated emission is less than that from the disordered surfaces which yield much higher cross sections for emission into evanescent LEED states. Apparently, the surface potential associated with a rough surface yields stronger matrix elements connecting bulk initial states with LEED-type final states.

We also note that the photon-energy dependence of the photoelectron cross section for the surface-state peak serves as an independent check on the Δ_1 and symmetry final band. The emission from a surface state is strongest at photon energies which permit transitions into a bulk final state near a zone boundary. We find that the surface-resonance peak is maximized for photon energies of approximately 14—16 eV where the final-state Δ_1 band intersects the zone edge at H.

Figure 7, which displays corresponding EDC's for p polarization, exhibits similar behavior; most of the peaks do not disperse with photon energy. There is evidence of emission from the two lower Δ_1 symmetry bands in the photon-energy range from 10 to 22 eV. These peaks disperse at lower photon energies where direct transitions to the Δ_1 symmetry final band are allowed ($h\nu < 12$ eV). At higher photon energies, the gap in the Δ_1 final band prohibits direct transitions, and the peaks appear stationary as surface-emission processes favor emission from the weakly dispersing portions of the Δ_1 band; this emission originates near the H point ($H_{12\uparrow}$ and $H_{12\downarrow}$). Additional evidence that these peaks are due to the lower $\Delta_{1\uparrow}$ and $\Delta_{1\downarrow}$ bands near H is based on the selection rules. No evidence of these peaks is apparent in the s-polarization data (Fig. 6) as required by the selection rules. These structures are therefore assigned to direct transitions from the $\Delta_{1\downarrow}$ and $\Delta_{1\uparrow}$ bands near H to the Δ_1 final band ($h\nu < 14$ eV) and to LEED final states ($h\nu \geq 14$ eV).

We have plotted in Fig. 9 our measured binding energies versus $k_\perp$ based on the free-electron band shown in Fig. 2. It is clear from these results that normal emission from the (100) surface does not provide a great deal of information about the binding energy and dispersion of the occupied bands along the Δ line. However, we have found that the Δ_1 symmetry final-band gap and other factors permit a rather complete study of surface states and surface resonances on Fe(100).[49]

C. Fe(111) normal emission

Electrons emitted along the [111] direction can probe both the Λ and F lines of the three-dimensional Brillouin zone. The Fe(111) surface has been investigated previous-
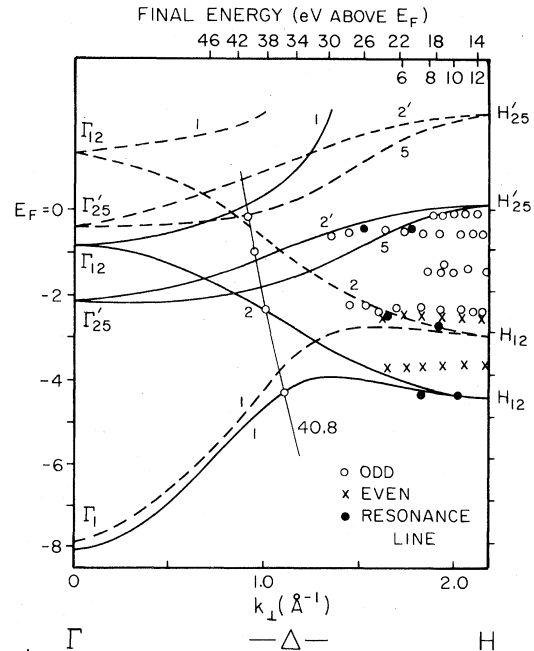

FIG. 9. Experimental results plotted over calculated bands along the Δ direction for ferromagnetic iron. Binding energies of even states are represented by $\times$, odd states by $\bigcirc$. The points which project into gaps at H based on assuming a free-electron final band are due to surface (nondirect) transitions from initial states near Γ.

ly by Eastman *et al.*[21] using angle-resolved photoemission and synchrotron radiation. The exchange splitting and band dispersion near P was determined using the direct-transition model. Figure 10 shows our normal-emission spectra for Fe(111) which were taken using unpolarized light from a resonance lamp incident at an angle of 45°. Using the same free-electron final band as Eastman *et al.*, which agrees quite well with the predicted F_1 symmetry final band (see Fig. 2), we have confirmed their determination of the binding energies at P. However, Eastman *et al.* concluded that photons with $h\nu \geq 10$ eV probe the F line even though the lower three symmetry bands were dispersing upward rather than downward as would be expected when going toward H along the F line. The higher-energy spectra in Fig. 10, particularly the 48.38-eV spectrum, show that substantial emission from the Λ line can be seen in this range. The inset in Fig. 10 shows the band structure of iron along the Λ and F lines. Using the same final band as Eastman *et al.*, we have plotted the experimental bands along F. To determine the relative contribution of emission from the Λ and F lines in this energy range will require additional experimental work using synchrotron radiation. The peak near E_F at 40.82 eV (which is shaded) appears to be very sensitive to surface conditions and may be caused by a surface state at $\overline{\Gamma}$.

D. Fe(100) off-normal emission

Off-normal photoemission provides a means of probing portions of the Brillouin zone which are not accessible in normal-emission geometry. Off-normal studies also provide a means of checking selected critical points deter-
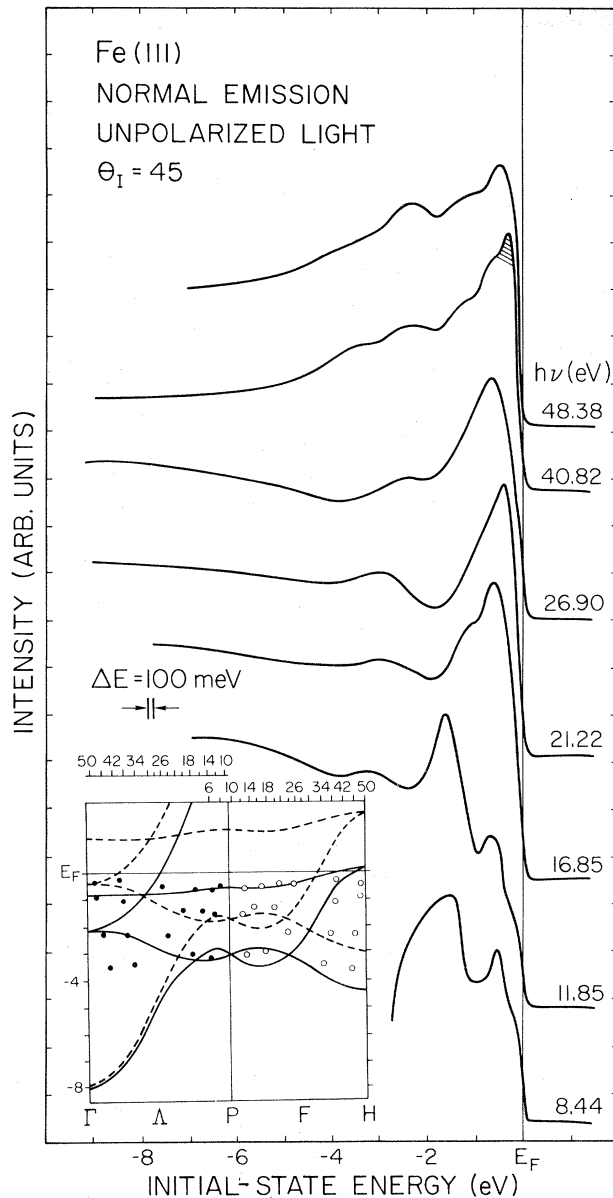
FIG. 10. Normal-emission EDC's for Fe(111). Unpolarized light from a resonance lamp is incident at 45°. Initial states and $k_\perp$ values along Λ are identified directly in the figure.

tion ($\overline{M}$ point). Once the final band has been determined, the specific point along a symmetry line probed at any given photon energy can also be determined. This forms the basis for consistency checks. For example, the Σ line is probed in normal emission from the (110) surface, and the D line is probed at the $\overline{M}$ point from the (110) surface. These lines intersect at N, and the binding energies at N can be determined from either crystal face.

The inner potential which places the final band for direct-transition photoemission from the (100) surface was determined in normal-emission experiments described in Sec. II B. Equations (1)–(7) and the inner potential can be used to calculate $k_\perp$ along the D line at a particular photon energy. These values of $k_\perp$ correspond in Figs. 11(b) to the intersection of the circles (which represent specific final-band energies above E_F) with the vertical line corresponding to a particular value of $k_{||}$ ($k_{||}=1.55$ Å^{-1} for the D line). Referring to Fig. 11(b), one can see that a photon energy of 22 eV places initial states having low binding energy (i.e., near E_F) at $k_{||}$ and $k_\perp$ values corresponding to the N point in the bulk Brillouin zone.

The calculated energy bands along the D line are shown in Fig. 13. Superimposed on the bands are points corresponding to the EDC's shown in Fig. 12 (and some additional points for EDC's which are not shown). The binding energies and band symmetries obtained from the photoemission data are in good agreement with the calculated bands. States of D_1 and D_4 symmetry are even in the (110) plane, and those of D_2 and D_3 symmetry are odd. Off-normal EDC's obtained using s-polarized light correspond to even initial states ($\vec{A}$ vector parallel to $k_{||}$) and those using p-polarized light correspond to odd initial states ($\vec{A}$ vector perpendicular to $k_{||}$).

EDC's taken at $\overline{M}$ using $h\nu=22$ eV locate several initial-state bands near N. The EDC for p polarization locates even-symmetry bands having binding energies of 0.80 eV ($D_{1\uparrow}$), 1.30 eV ($D_{4\downarrow}$), and 3.50 eV ($D_{4\uparrow}$ and $D_{1\downarrow}$ unresolved). Figure 13 indicates accurate $k_\perp$ values for these peaks along D. A fourth even-symmetry band $D_{1\uparrow}$ is obscured by the O $2p$ level in the spectrum shown in Fig. 13 but is resolved in EDC's obtained from clean surfaces (not shown). The lower $D_{1\uparrow}$ peak lies at 3.80 eV below E_F at $\overline{M}$. The EDC for s polarization locates the flat odd-symmetry band $D_{2\uparrow}$ at 0.70 eV below E_F. A second peak at 3.2 eV below E_F and the shoulder at 1.5 eV appear to be caused by indirect transitions from points near P. Other spectra (not shown) taken at $h\nu=40.82$ and 48.38 eV exhibits three distinct peaks which correspond to direct transitions at $k_\perp$ values near P. The position of these peaks agree very well with the binding energies of $P_{3\uparrow}$, $P_{4\downarrow}$, and $P_{4\uparrow}$ determined from the (111) face.

Several interesting features associated with off-normal-emission studies can be identified by considering the normal-emission spectra in Figs. 6 and 7 and the off-normal-emission spectra in Fig. 12. As we discussed in Sec. II B, characteristic features of the band structure along the Δ line cause difficulties in mapping bulk bands. The Δ_1 final band is only suitable for studying the spin-split Δ bands near H, and at H_{15} it changes to Δ_5 (odd) symmetry. In off-normal geometry along the [010] and [110] directions, the Δ_5 band can be decomposed into odd-

mined in normal-emission experiments. Figure 11(a) illustrates the bulk Brillouin zone for a bcc crystal and the accompanying inset [11(b)] represents cuts through the bulk Brillouin zone along the [011] directions parallel to the (100) axis. The surface Brillouin zone for the (100) surface is also shown in Fig. 11(a) with three high-symmetry points represented by $\overline{\Gamma}$, $\overline{X}$, and $\overline{M}$. Two of these points correspond to high-symmetry lines in the bulk Brillouin zone represented by Δ and D lines.

By selecting appropriate emission angles, θ [using Eq. (5)], one can probe particular points in the surface Brillouin zone and the corresponding lines in the bulk Brillouin zone. The EDC's displayed in Fig. 12 correspond to $k_{||}=1.10$ Å along the [010] direct ($\overline{X}$ point on the surface Brillouin zone) and $k_{||}=1.55$ Å^{-1} along the [110] direc-

(100) SURFACE
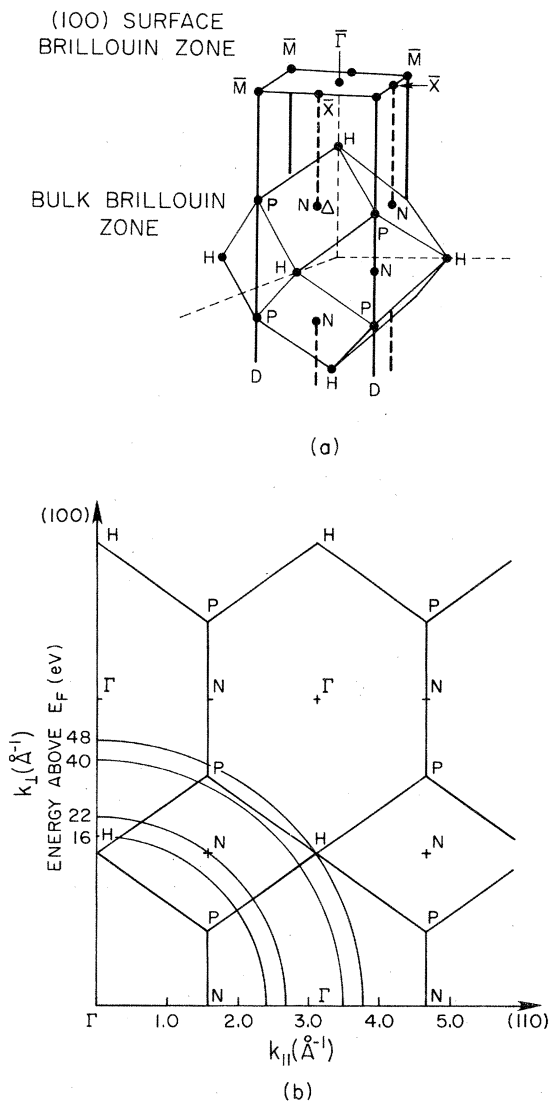BRILLOUIN ZONE

BULK BRILLOUIN
ZONE

(a)

(b)

FIG. 11. (a) Bulk Brillouin zone for a bcc lattice and surface Brillouin zone for the (100) surface. (b) Cut through the bulk Brillouin zone along the (110) direction. Circles show location in k space associated with final-band energies of 16, 22, 40, and 48 eV above E_F.

and even-component basis functions which permit observations of direct transitions. More specifically, along the $z = y$ (110) plane, the even and odd Δ_5 basis functions are $z - y, xz - yz$ and $z + y, xz + yz$, respectively, and along the $z = 0$ plane (001), the even and odd Δ_5 basis functions are z, xz and y, xy. Inspection of final bands along the D line (off-normal emission from the 100 surface at $\overline{M}$) shown in Fig. 2 shows that there is a Δ_1 (even) symmetry final band which agrees fairly well with the free-electron band characterized by the (100) surface inner potential U_0. The major peaks seen in Fig. 13 result from direct transitions, and the intensity of these peaks is roughly three times the intensity of corresponding peaks in normal-emission EDC's which result from the surface-emission mechanism.
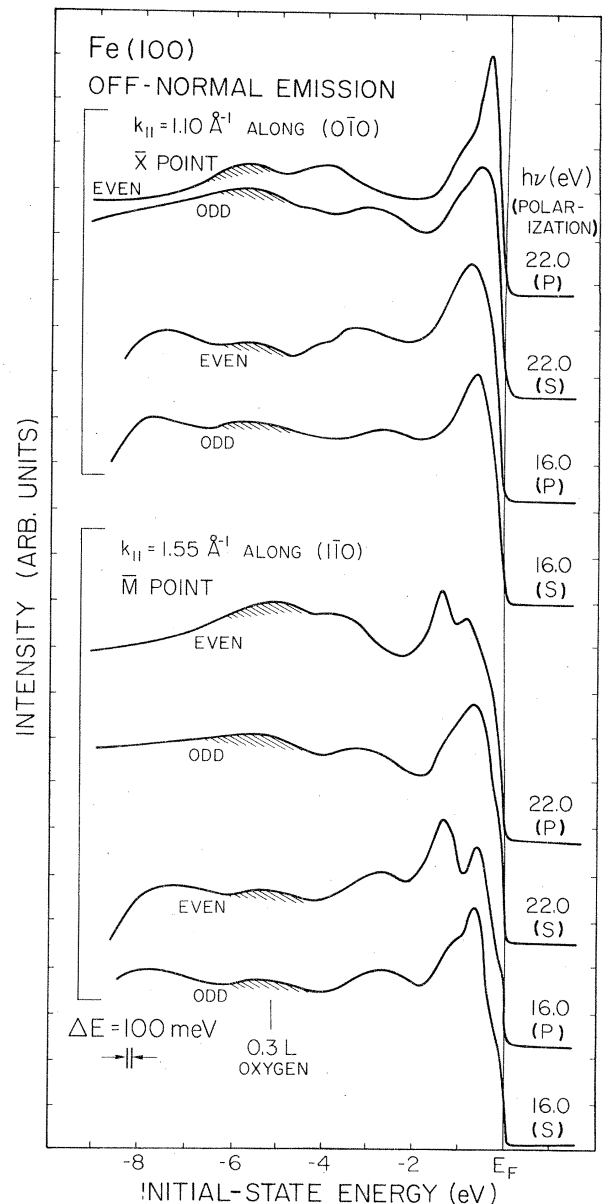

FIG. 12. Off-normal emission EDC's for Fe(100). Top panel corresponds to the X point in the surface Brillouin zone, bottom panel corresponds to the $\overline{M}$ point. Shaded peaks identify oxygen $2p$ level (0.3 monolayer). Polarization and photon energies are identified to the right of each EDC. p-polarization ($\phi_I = 45$) spectra correspond to $\vec{A}$ perpendicular to the plane determined by $k_{||}$ and the sample normal.

IV. DISCUSSION

Table II summarizes the critical-point binding energies, referenced to the Fermi energy, that we have determined from our angle-resolved photoemission data. These experimental results are compared with recent calculations for ferromagnetic iron by several groups. We again point out that the calculated energies represent ground-state eigenvalues based on one-electron band calculations whereas our measured binding energies correspond to an excitation
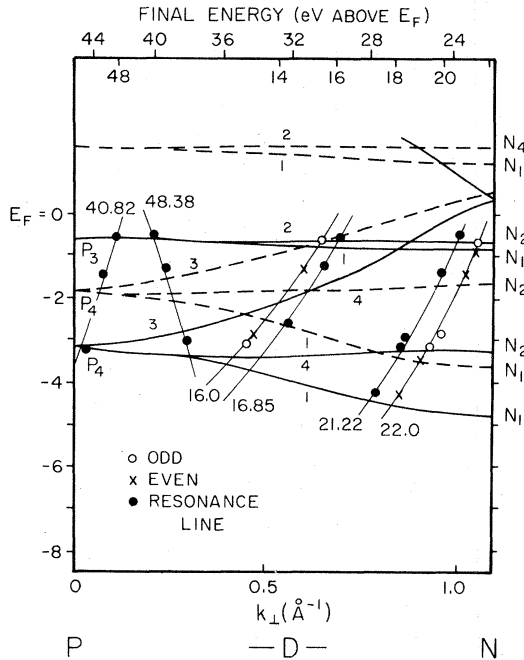
FINAL ENERGY (eV ABOVE E_F)

FIG. 13. Experimental results plotted over calculated bands along the D direction for ferromagnetic iron. Binding energy of even states are represented by $\times$, odd states by $\bigcirc$. Data obtained using resonance lines are represented by $\bullet$. Bands labeled D_1 and D_4 are even; those labeled D_2 and D_3 are odd. Photon energies correspond to the points as indicated.

lieved to constitute the most important correction required to compare one-electron ground-state energies with photoemission results. In the Introduction, it was pointed out that the bandwidth and exchange splitting of Ni determined from angle-resolved photoemission measurements was in striking disagreement with state-of-the-art calculations. The discrepancies are significant especially when considered in relation to results for Cu and it is the Coulomb correlation effects which apparently account for the disagreement. We first neglect these effects and use the results summarized in Table II to compare band energies and the exchange splitting for Fe throughout the three-dimensional Brillouin zone in the same spirit in which calculations and experiments have been compared for Cu and Ni. We return to the questions regarding correlation effects later.

We first consider the calculated d-band width of Fe. The lowest-lying d band has been determined at several points in the Brillouin zone: $\Gamma'_{25\uparrow}$, $P_{4\uparrow}$, $H_{12\uparrow}$, and $N_{1\uparrow}$. For the purpose of the present discussion, we choose to define the d-band width as the energy difference between E_F and the lowest-lying band having d character. The average difference between our experimental binding energies and the calculated energies of Callaway and Wang for these four points is approximately 10%. The calculation of Callaway and Wang appears to underestimate d-state binding energies near E_F by a few percent ($\Gamma'_{25\uparrow}$ and $P_{4\uparrow}$) and overestimate d-state binding energies away from E_F by a little more ($N_{1\uparrow}$ and $H_{12\uparrow}$). The sp-band minimum $\Gamma_{1\uparrow\downarrow}$ appears to be accurately determined by their calculation. Of the three calculations represented in Table II the bands obtained by Callaway and Wang using the von Barth—Hedin (vBH) potential appear to yield the best overall agreement with our experimental results. All three

spectrum of the solid as viewed by the photoemission process. This fact must be considered in comparing the experimental and calculated band energies represented in Table II. Effects of Coulomb correlations[30,31,50] are be-

TABLE II. Critical-point binding energies and exchange splitting determined by experiments and comparison with three recent calculations. All values are in eV measured from the Fermi energy.

	Jansen	Moruzzi	vBH	Callaway KS	$\alpha=0.64$	Expt.
$\langle\Gamma_{1\uparrow\downarrow}\rangle$	8.93	8.42	8.12	8.13	8.29	8.15±0.20
$\Gamma_{25'\uparrow}$	2.50	2.48	2.25	2.32	2.32	2.35±0.10
$\Gamma_{12\uparrow}$	1.44	0.97	0.86	0.94	0.92	0.78±0.10
$\Gamma_{25'\downarrow}$	0.45	0.45	0.43	0.02	0.15	0.27±0.05
$H_{12\uparrow}$	5.60	5.17	4.50	4.57	4.61	3.80±0.30
$H_{12\downarrow}$	3.43	3.71	2.99	2.71	2.87	2.50±0.30
$P_{4\uparrow}$	3.61	3.50	3.17	3.23	3.26	3.20±0.10
$P_{3\uparrow}$	1.17	0.68	0.53	0.73	0.71	0.60±0.08
$P_{4\downarrow}$	2.18	1.95	1.83	1.59	1.75	1.85±0.10
$N_{1\uparrow}$	5.52	5.24	4.75	4.80	4.86	4.50±0.23
$N_{2\uparrow}$	3.73	3.65	3.27	3.34	3.36	3.00±0.15
$N_{1\uparrow}$	1.25	0.94	0.86	0.94	0.92	0.70±0.08
$N_{4\uparrow}$	1.21	0.72	0.69	0.77	0.74	0.70±0.08
$N_{1\downarrow}$	4.18	3.92	3.60	3.40	3.57	3.60±0.20
$N_{2\downarrow}$	1.89	1.82	1.62	1.26	1.40	1.40±0.10
Δ_{exc}						
$\Gamma_{25'}$	2.05	2.03	1.82	2.30	2.17	2.08±0.10
H_{12}	2.17	1.46	1.51	1.86	1.74	1.30±0.30
P_4	1.43	1.55	1.34	1.64	1.51	1.35±0.10
N_2	1.84	1.83	1.65	2.08	1.96	1.60±0.15

of the calculations give much better overall agreement for bandwidth (as defined here) than was found to be the case for Ni, even before taking into account Coulomb correlation effects.

The calculated exchange splitting of Fe also appears to be in significantly better agreement with experimental results than that found for Ni. The exchange splitting is determined accurately at Γ, P, H, and N in the three-dimensional Brillouin zone: $E_{\Gamma'_{25\uparrow}} - E_{\Gamma'_{25\downarrow}} = 2.08 \pm 0.10$, $E_{P_{4\uparrow}} - E_{P_{4\downarrow}} = 1.35 \pm 0.10$, $E_{H_{12\uparrow}} - E_{H_{12\downarrow}} = 1.30 \pm 0.30$, and $E_{N_{2\uparrow}} - E_{N_{2\downarrow}} = 1.60 \pm 0.15$ eV. It is clear that the exchange splitting depends on the location in the three-dimensional Brillouin zone, and that it can change rather rapidly along a symmetry line. This is apparent along the Δ, Σ, and Λ lines of the Brillouin zone (see Fig. 2) where the s-p band originating from Γ_1 exhibits very little exchange splitting at Γ, but is split by over 1 eV at H, P, and N where it hybridizes with d-symmetry bands. The evolution of the splitting along part of the Σ line can be seen in photoemission spectra shown in Fig. 3. There appears to be two distinct mechanisms which can account for the observed variation in the exchange splitting throughout the Brillouin zone. Mixing of sp and d wave functions probably accounts for the rapid increase in the splitting along the band originating at Γ (where the band has pure s symmetry) as it disperses upward toward the zone boundary. In addition, it is well known that the exchange splitting of d bands is dependent on energy due to the contraction of wave functions of antibonding states near the top of the band and expansion of wave functions of the low-lying bonding states. This effect accounts for the Stoner parameter being larger at the top of the band than at the bottom in Fe, and thus results in the minority-spin d band of Fe (here we refer to the total bandwidths including filled and empty states) being about $\frac{1}{2}$ eV wider than the majority-spin band.[51]

A principle objective of the calculation of Fe by Callaway and Wang was to study how spin-polarized band calculations using a local-exchange potential are affected by the inclusion of correlation effects in the potential. In their paper they compare explicitly specific differences between results obtained using local exchange potential with $\alpha = \frac{2}{3}$ [Kohn-Sham (KS)] and $\alpha = 0.64$, and the vBH exchange-correlation potential. All three results are represented in Table II. These differences include a slightly narrower d-band width (0.1 eV difference), a smaller exchange splitting (0.5 eV near the top of the band), and a significant difference in the width of the minority-spin bands (6.4 eV for KS and 6.1 eV for vBH). Also, the sp-band splitting is apparently about twice as large at Γ (0.2 eV) for the vBH potential than for the KS potential. Based on these general differences and specific values in Table II we can say that the vBH potential yields ground-state energies which are in closest agreement with our experimentally determined critical-point binding energies.

We briefly comment on the other two calculations represented in Table II. The semiempirical calculations of Jansen and Mueller[11] appear to overestimate the energy of both sp and d bands. These calculations rely on experimental results (primarily de Haas–van Alphen data) to

construct a one-electron potential. The self-consistent ab initio calculations of Moruzzi et al.[1] incorporate exchange and correlation in the local one-electron potential, and also yield results which are also in good agreement with experiment. The bands calculated by Moruzzi et al. appear to yield comparable accuracy with the results of Callaway and Wang for bands near E_F, but apparently are less accurate for states away from E_F. For example, the s-p—band minimum is about 0.25 eV lower than that shown by experiment, and values near H appear to be considerably lower than those measured by experiment. Clearly, all of the recent calculations for iron are in much better agreement with experimental results than for nickel. A recent ab initio calculation by Greenside and Schlüter[52] of the electronic properties of ferromagnetic iron illustrates application of pseudopotentials with a local exchange and correlation potential. Results for two values of lattice constant are reported: $d = 5.4$ and 5.2 a.u. Ground-state energies obtained for $d = 5.4$ a.u. appear to have about the same good agreement with our data as that obtained by Callaway and Wang near E_F, and similar slightly larger errors away from E_F just as obtained by Moruzzi et al. For example, Greenside and Schlüter cite (for $a = 5.4$ a.u.) $E_{N_{1\uparrow}} = 4.70$, $E_{N_{1\downarrow}} = 4.06$ (lower bands), and $E_{N_{1\uparrow}} = 0.75$, $E_{N_{1\downarrow}} = 0.07$ eV (upper bands). The s-p—band minimum $E_{\Gamma_{1\uparrow\downarrow}}$(average) $= 8.52$ eV is larger than both the Callway and Moruzzi results.

Our study of the bulk electronic properties of Fe has provided the basis for detailed worked on the surface electronic properties including surface states on high-symmetry surfaces and surface magnetic properties. This work will be presented in detail in a separate paper.[53] We can state here that surface states and surface resonances play an important role in electron-emission processes from Fe surfaces, especially the Fe(100) surface.

We now return briefly to questions regarding Coulomb correlation effects. The measured binding energies in Table II averaged over all critical points determined by the experiment are about 8% lower than the theoretical ground-state energies. A more detailed analysis shows that the lower binding energies ($E_B < 1.0$ eV) tend to disagree on the average about 10%, and the higher binding energies ($E_B > 3.0$ eV) disagree on the average by about 7%. A 10% error is significant in view of the rather generous error bars we have stated for our experimentally determined binding energies. Treglia et al.[50] have considered effects of Coulomb correlations on energy bands in ferromagnetic Ni, Co, and Fe. Their analysis for Ni yields a 30% reduction in ground-state energies and the "corrected" ground-state band structure is then found to be in good agreement with photoemission results. Their analysis for Fe yields a smaller correction, amounting to a 10% d-band width narrowing of calculated ground-state bands. The direction and magnitude of their predicted correction is just what is required to bring the ground-state calculations to within experimental error (averaged over all critical points determined) of our data.

Based on our results we can also offer a few comments on how energy-resolved spin-polarized photoemission experiments, which have now been shown to be feasible,

could help improve and verify the results obtained here. The Fe(111) and Fe(110) surfaces are less susceptible to surface emission which can complicate data analysis and appear to be good candidates for spin-polarized photo-emission studies of bulk magnetic bands. Several portions of the three-dimensional Brillouin zone of iron present opportunities to study exchange split bands, and these bands are accessible at photon energies and from crystal faces which permit direct transitions to bulk final-state bands with little interference from surface-emission effects. Specific examples which use normal-emission geometry are the Γ point studied from the (110) surface and the P point studied from the (111) surface. Spin-polarized emission studies of these cases should be able to provide a direct and unambiguous consistency check on several specific results given in Table II, and should also be able to help answer important questions regarding the temperature dependence of exchange splitting.

V. CONCLUSION

We have presented direct measurements of the exchange splitting, band dispersion, and critical-point binding energies of the bulk bands of ferromagnetic iron. The results indicate that the electronic structure of ferromagnetic iron calculated self-consistently based on local-exchange and correlation potentials is substantially correct. Surface-photoemission processes involving both bulk and surface states play an important role in photoemission from iron surfaces. These features present some problems in studying bulk electronic states in iron, particularly for the (100) surface. But, in general, the direct-transition model of photoemission appears to constitute an adequate basis for analyzing angle-resolved photoemission data for Fe. Coulomb correlation effects do not play a decisive role in reconciling measured binding energies with ground-state energies as in the case of Ni, but the sign and magnitude of estimated correlation effects are exactly what is required to account for the discrepancy between our data and the best energy-band calculations. The results strengthen the case for the importance of correlation effects in transition metals.

[1]V. L. Moruzzi, J. F. Janak, and A. R. Williams, *Calculated Electronic Properties of Metals* (Pergamon, New York, 1978).

[2]G. A. Burdick, Phys. Rev. 129, 138 (1963).

[3]J. F. Janak, A. R. Williams, and V. L. Moruzzi, Phys. Rev. B 6, 4367 (1972); 11, 1522 (1975).

[4]C. S. Wang and J. Callaway, Phys. Rev. B 15, 298 (1977).

[5]F. Smulowicz and D. M. Pease, Phys. Rev. B 17, 3341 (1978).

[6]J. W. D. Connolly, Phys. Rev. 159, 415 (1967).

[7]J. Callaway and C. S. Wang, Phys. Rev. B 16, 2095 (1977); R. A. Tawil and J. Callaway, *ibid.* 7, 4242 (1973); M. Siugh, C. S. Wang, and J. Callaway, *ibid.* 11, 287 (1975).

[8]S. Wakoh and J. Yamashita, J. Phys. Soc. Jpn. 21, 1712 (1966).

[9]K. J. Duff and T. P. Das, Phys. Rev. B 3, 192 (1971).

[10]M. Yasui, E. Hayashi, and M. Shimizu, J. Phys. Soc. Jpn. 34, 396 (1973).

[11]H. J. F. Jansen and F. M. Mueller, Phys. Rev. B 20, 1426 (1979); H. J. F. Jansen, Ph.D. thesis, University of Groningen, The Netherlands, 1981 (unpublished).

[12]Recent review articles include B. Feuerbacher and R. F. Willis, J. Phys. C 9, 169 (1976); H. D. Hagstrum and J. E. Rowe, *Experimental Methods in Catalytic Research* (Academic, New York, 1976), Vol. III; E. W. Plummer and W. Eberhardt, Chem. Phys. 49, 533 (1983).

[13]P. Thiry, D. Chandesris, J. Lecante, C. Guillot, R. Pinchaux, and Y. Petroff, Phys. Rev. Lett. 43, 82 (1979).

[14]E. Dietz and D. E. Eastman, Phys. Rev. Lett. 41, 1674 (1978); E. Dietz and F. J. Himpsel, Solid State Commun. 30, 235 (1979).

[15]J. A. Knapp, F. J. Himpsel, and D. E. Eastman, Phys. Rev. B 19, 4952 (1979).

[16]W. Eberhardt and E. W. Plummer, Phys. Rev. B 21, 3245 (1980), and references therein.

[17]F. J. Himpsel, J. A. Knapp, and D. E. Eastman, Phys. Rev. B 19, 2919 (1979).

[18]P. Heimann and H. Neddermeyer, Phys. Rev. B 18, 3537 (1978).

[19]S. D. Kevan, P. S. Wehner, and D. A. Shirley, Solid State Commun. 28, 517 (1978).

[20]A. Schultz, R. Courths, H. Schulz, and S. Hufner, J. Phys. F 9, L41 (1979).

[21]D. E. Eastman, F. J. Himpsel, and J. A. Knapp, Phys. Rev. Lett. 44, 95 (1980).

[22]A. M. Turner and J. L. Erskine, Phys. Rev. B 25, 1983 (1982).

[23]I. D. Moore and J. B. Pendry, J. Phys. C 11, 4615 (1978).

[24]I. D. Moore, Solid State Commun. 32, 907 (1979).

[25]R. Clauberg, Phys. Rev. B 27, 4644 (1983).

[26]W. Eib and S. F. Alvarado, Phys. Rev. Lett. 37, 444 (1976).

[27]E. Kisker, W. Gudat, M. Campagna, E. Kuhlmann, H. Hopster, and I. D. Moore, Phys. Rev. Lett. 43, 966 (1979).

[28]W. Gudat, E. Kisker, E. Kuhlmann, and M. Campagna, Phys. Rev. B 22, 3282 (1980); E. Kisker, W. Gudat, E. Kuhlmann, R. Clanberg, and M. Campagna, Phys. Rev. Lett. 45, 2053 (1980).

[29]R. Clauberg, W. Gudat, E. Kisker, and E. Kuhlmann, Z. Phys. B 43, 47 (1981).

[30]D. R. Penn, Phys. Rev. Lett. 42, 921 (1979).

[31]A. Liebsch, Phys. Rev. Lett. 43, 1431 (1979); Phys. Rev. B 23, 5203 (1981).

[32]G. Borstel, H. Przybylski, M. Neumann, and M. Wöhlecke, Phys. Rev. B 25, 2006 (1982).

[33]J. L. Erskine, Phys. Rev. Lett. 45, 1446 (1980).

[34]D. G. Dempsey and L. Kleinman, Phys. Rev. Lett. 39, 1297 (1977); D. G. Dempsey, W. R. Grise, and L. Kleinman, Phys. Rev. B 18, 1270 (1978).

[35]W. Kohn and L. J. Sham, Phys. Rev. 140, A1133 (1965).

[36]L. Hedin and B. I. Lundqvist, J. Phys. C 4, 2064 (1971).

[37]J. F. Janak, Phys. Rev. B 9, 3985 (1974).

[38]H. A. Stevens, M.A. (Physics) thesis, University of Texas at

Austin, 1983 (unpublished).

[39]G. K. Ovrebo and J. L. Erskine, J. Electron. Spectrosc. Relat. Phenom. <u>24</u>, 189 (1981).

[40]H. A. Stevens, A. W. Donoho, A. M. Turner, and J. L. Erskine, J. Electron. Spectrosc. Relat. Phenom. <u>32</u>, 327 (1983).

[41]J. Hermanson, Solid State Commun. <u>22</u>, 9 (1977).

[42]W. Eberhardt and F. J. Himpsel, Phys. Rev. B <u>21</u>, 5572 (1980).

[43]T. C. Chiang, J. A. Knapp, M. Aono, and D. E. Eastman, Phys. Rev. B <u>21</u>, 3513 (1980); W. Eberhardt and E. W. Plummer, Phys. Rev. B <u>21</u>, 3245 (1980).

[44]E. Colavita, M. De Crescenzi, L. Papagno, R. Scarmozzino, L. S. Caputi, R. Rosei, and E. Tosatti, Phys. Rev. B <u>25</u>, 2490 (1982).

[45]B. Egert and G. Panzner, J. Phys. F <u>11</u>, L233 (1981).

[46]J. H. Weaver, E. Colavita, D. W. Lynch, and R. Rosei, Phys. Rev. B <u>19</u>, 3850 (1976).

[47]Shang-Lin Weng, E. W. Plummer, and T. Gustaffson, Phys. Rev. B <u>18</u>, 1718 (1978).

[48]A. M. Turner, Yu-Jeng Chang, and J. L. Erskine, Phys. Rev. Lett. <u>48</u>, 348 (1982).

[49]A. M. Turner, and J. L. Erskine, Phys. Rev. B <u>28</u>, 5628 (1983).

[50]G. Treglia, F. Ducastelle, and D. Spanjaard, J. Phys. <u>43</u>, 341 (1982).

[51]O. Gunnarsson, Physica <u>91B</u>, 329 (1977).

[52]H. S. Greenside and M. A. Schlüter, Phys. Rev. B <u>27</u>, 3111 (1983).

[53]A. M. Turner and J. L. Erskine (to be published).